VALIDATION OF THE ESA STATISTICAL RE-ENTRY MODELING TOOL DRAMA ON GROUND-BASED OPTICAL DATA

Matej Zigo[(1)], Daniela Bartková[(2)], Jiří Šilha[(1,2)], Juraj Tóth[(2)], Stijn Lemmens[(3)], and Beatriz Jillet[(3)]

[(1)] *Astros Solutions s.r.o., Nad Lúčkami 3141/35, 84 105, Bratislava, Slovakia*
[(2)] *Faculty of Mathematics, Physics, and Informatics, Comenius University Bratislava, Mlynska dolina, 842 48 Bratislava, Slovakia*
[(3)] *ESA/ESOC, Space Debris Office, Robert-Bosch-Strasse 5, DE-64293 Darmstadt, Germany*

ABSTRACT

Following the re-entry of the Chinese Long March (CZ-3B) launcher upper stage in 2020, Astros Solutions s.r.o., in collaboration with Comenius University in Bratislava, has embarked on an ambitious project to reconstruct the event and refine physical re-entry models using this extraordinary dataset. A major focus of this effort is validating the ESA's DRAMA toolkit—a sophisticated statistical re-entry modeling tool capable of simulating re-entry trajectories, parent body fragmentation, and assessing on-ground risk.

Leveraging their expertise in meteor physics and dynamics, Comenius University conducted an in-depth physical analysis, adapting their modeling tools to account for artificial materials. This enabled them to reconstruct the event with remarkable precision and extract critical parameters characterizing the re-entry. In parallel, Astros Solutions employed minimal initial data to set up input parameters for DRAMA, using its statistical models to generate a comprehensive event reconstruction.

This work presents both methodologies in detail, showcasing a comparative analysis of DRAMA's statistical reconstructions alongside the physical modeling results from the analysis of the event observations. Our findings highlight the strengths and limitations of DRAMA through validation against purely physical methods, marking a significant step forward in re-entry event modeling and impact prediction.

Keywords: Re-entry events, DRAMA, Modeling, AMOS, Space Debris.

1. INTRODUCTION

Re-entry events are caused by artificial objects such as defunct satellites, upper stages, fragmentation debris, cargo ships, etc. These objects, after losing altitude due to atmospheric drag, re-enter the Earth's atmosphere at high velocities, undergoing intense heating, ablation, and potential fragmentation. The physics behind these events is similar to that of meteors, which are commonly tracked by astronomers using all-sky cameras equipped with wide field-of-view lenses. The primary distinction between natural meteoroid entries and artificial object re-entries lies in their velocity, material composition, and expected survival of fragments upon impact.

Ground-based optical systems play a crucial role in monitoring and analyzing re-entry events. All-sky cameras, initially designed for meteor detection, have proven to be highly effective in capturing artificial object re-entries due to their ability to continuously survey large portions of the sky. The data collected from these systems enable precise trajectory reconstruction, fragmentation analysis, and impact location prediction. The AMOS (All-sky Meteor Orbit System) network, operated by Faculty of Mathematics, Physics and Informatics, Comenius Univ. Bratislava (FMPI), is among the few ground-based astronomical systems capable of detecting and characterizing both meteoroid and artificial re-entry events. By leveraging multi-station observations, these systems provide valuable insights into the dynamics of uncontrolled re-entries, contributing to the improvement of re-entry models and risk assessment strategies.

On October 25th, several services, including Space-Track.org, operated by the US 18th Space Defense Squadron (18th SDS), and the European Union Space Surveillance and Tracking network (EUSST), operated by the EUSST Consortium at the time, predicted that the CZ-3B (COSPAR no. 2008-055B, NORAD 33415) would decay that day, most likely above the Pacific Ocean. Later, the 18th SDS confirmed that the re-entry occurred on 2020-10-25 at 08:02:00 UTC, with the re-entry point at 19.6° North latitude and 161.4° West longitude, which corresponds to a location a few hundred kilometers west of the Hawaiian Islands.

Figure 1: AMOS sensors which captured the re-entry event CZ-3B on Manuakea (left) and Haleakala (right) observatories in Hawaii.

1.1. AMOS recordings

The primary data source for this study consisted of video recordings that captured the re-entry event over the Hawaiian Islands. The CZ-3B re-entry event on October 25th was recorded by three cameras of the AMOS (All-Sky Meteor Orbit System) network (Figure 1). These observations provided crucial optical data for trajectory reconstruction, fragmentation analysis, and impact location estimation.

AMOS operates as a ground-based optical network designed primarily for meteor detection. AMOS cameras are fully automated and do not require human interaction during the detection of meteors, as they utilize an event-based triggering system optimized for transient luminous phenomena. However, the detection of artificial re-entries presents unique challenges. Due to their often slower angular velocity, varying brightness, and extended luminous phases compared to meteors, human-in-the-loop intervention might be required to ensure successful tracking and classification of artificial objects.

The data reduction process was carried out using available meteor processing software and established methodologies. This involved background subtraction, astrometric calibration, and trajectory triangulation, followed by brightness curve analysis to assess ablation and fragmentation characteristics. By leveraging multi-station observations, the extracted data were used to refine re-entry modeling and validate predictive simulations [3].

The observing conditions and location of the re-entry event were very suitable for the AMOS stations on Hawaii (Table 1). Particularly, the re-entry light trajectories crossed through the zenith of Haleakala station (Figure 2, left). The event moved closer to the horizon of the Manuakea station (Figure 2, right). A section of the flight also moved throughout the FOV of the higher-resolution spectral camera at the Manuakea station.

The different perspectives of the event presented a challenge for the geometric reconstruction of the re-entry fragment cloud and identification of individual fragments from both stations. The first main goals of our analysis of the all-sky images of the re-entry event was to measure the trajectories, beginning and terminal heights and speeds of the observed fragments.

Table 1: AMOS network sensors installed at Hawaii and their geographical locations.

Station code	**HK**	**MK SPEC-MK**
Station name	**Haleakala, Hawaii**	**Maunakea, Hawaii**
Longitude [deg]	-156.256	-155.477
Latitude [deg]	20.707	19.824
Altitude [m]	3068	4126
Operation start [m/y]	09/2018	09/2018

Figure 2: Left: Composite image of the CZ-3B reentry event of October 25th 2020 in the FOV of the AMOS camera at the Haleakala station in Hawaii. Right: Composite image of the CZ-3B reentry event of October 25th 2020 in the FOV of the AMOS camera at the Manuakea station in Hawaii.

Approximately one minute before the light trajectories of re-entry fragments were observed an explosion, which appears to be linked with the event, was captured by AMOS system on Haleakala. Therefore, an effort was made to extrapolate the re-entry trajectories back to the explosion point and measure the position of the upper stage explosion. The AMOS spectrograph additionally captured a faint emission spectrum of the brightest fragment.

2. DATA REDUCTION

AMOS-Capture software (Figure **??**), a custom program originally developed for the efficient detection and tracking of meteors captured by the AMOS network, was used for detecting and tracking the fragments created during the CZ-3B re-entry. The software requires precise information about the camera's exact location, its field of view, and various parameters such as resolution, frame rate, pixel size, and pixel saturation levels.

Detection, positioning, and intensity calculations of background stars are performed using a similar approach. The rectangular positions and intensities of these stars are essential for the astrometric and photometric reduction of the recordings. Since each fragment of the re-entry must be tracked individually, and in this case, the fragments were clustered in a relatively compact structure (Figure 2), it was essential to mask other fragments out of the

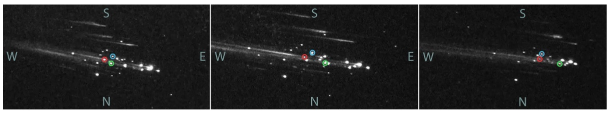

Figure 3: Changing perspective of the CZ-3B re-entry cluster captured by the all-sky AMOS camera at Haleakal's in three different chronologically ordered moments in time. The colored circles mark three fragments whose apparent position within the cluster changes. While the red and blue fragments stay close to each other, changing their relative position a little, the green one crosses from the center of the cluster to the front. This is caused by the change of perspective, not because it has a higher velocity.

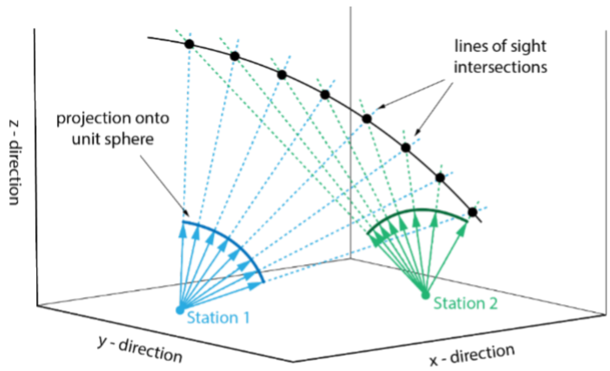

Figure 4: Illustration of direct triangulation approach to reconstruction of non-linear trajectory of an object moving through the Earth's atmosphere.

video recordings, leaving a single fragment visible to prevent undesired detections.

Since at least two-station position measurements are needed for the trajectory estimation to exploit the triangulation, each fragment with measured positions must be associated between two recordings obtained from two different locations. It turned out that the best tool for the association so far is the human eye, trained to recognize the spatial character of a moving object from changing perspective. This is known as the effect of parallax. Figure 3 depicts the scenario, when the fragments are associated within the same recording.

Custom methods for trajectory estimation in meteor physics assume linear trajectory, which may not be the case for re-entering artificial objects, as the gravitational pull is more pronounced for geocentric velocities. Hence, a direct triangulation approach was utilized for the CZ-3B re-entry fragments as shown in Figure 4.

Finally, seventeen fragments have been associated within the same recording and between two recordings acquired from two different stations. For these the 3D trajectory was constructed. In Figure 5 is plotted side view of the seventeen fragments, which were associated with the relative downrange to fragment F0-F0 as a function of elevation. For the time of observation 2020-10-25

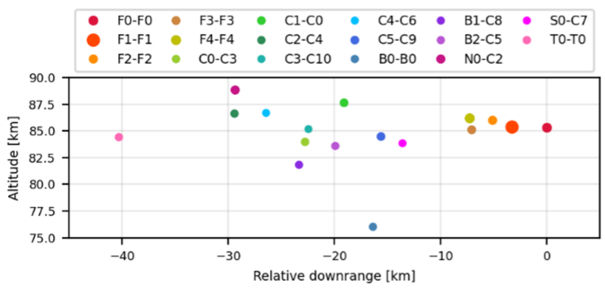

Figure 5: Side view of the fragments' relative positions in respect to the front fragment F0-F0 at 2020-10-25 08:02:02.000 UTC. Circles sizes corresponds to mean absolute magnitude of the fragments. Marker size is inversely proportional to the mean absolute magnitude of the given fragment (lower magnitude $\rightarrow$ higher brightness). The pair F1-F1 has the lowest mean absolute magnitude (1.392 mag).

08:02:02.000 UTC the fragmentation cloud's length was about 40 km long, its height was around 15 km and it covered 0.35 deg in geodetic longitude and 15 deg in latitude.

3. EVENT MODELING AND RECONSTRUCTION

To get a reasonable impact area estimate, the luminous trajectory was followed up by dark phase simulation, using software presented and described in [14]. Input parameters and initial conditions (terminal point) for individual fragments were set as presented in Table 2. The terminal velocity $v_T = 3km/s$ is the same for each fragment, as it is assumed that the terminal point is reached when the speed drops under this value.

For meteoroids, only objects with mass over 1.5×10^{-8}kg ($\sim 100\mu m$, approximately the size of a dust grain) are usually considered. In this case, the final masses of the fragments resulted to be either more than 10^{-3} kg or less than 10^{-5} kg, which implies the fragments essentially burned up and did not survive the ablation. The simulation was terminated when the object's altitude reached zero (impact).

Fragment B0-B0 is a special case. Due to the low value of the ablation coefficient resulting from the optimization using the triangulated trajectory, basically no mass loss is simulated and thus the fragment reaches the terminal point and impacts the surface. However, in AMOS-MK video recording, this fragment seems to shatter with a bright flare (Figure 6) after which the main sub-fragment seems to continue falling. The flare can be seen in the fragment's light curve (Figure 7). Unfortunately, since this was not observed with AMOS-HK, the triangulated trajectory does not reach this part and therefore cannot be compared with the simulation. Moreover, the model used for the simulation assumes a non-fragmenting sin-

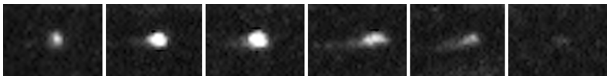

Figure 6: Flare of fragment B0-B0 as seen in the AMOS-MK video recording.

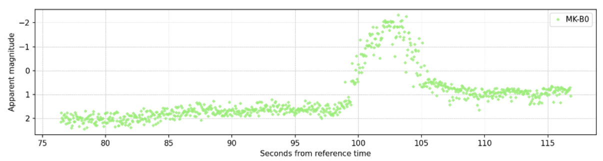

Figure 7: Apparent magnitude of fragment B0-B0 measured from AMOS-MK station.

gle body. The results presented in Table 8 should be taken with caution.

Fragments F0-F0 and F1-F1 most probably did not demise, at least not at the time as simulated. Regarding the fragments surviving in the simulation, there are two large and heavy pieces: F2-F2 and F3-F3, with high kinetic energies at the impact. Total surviving mass adds up to approximately 152 kg, which is around 5% of the dry mass (2800 kg) of the CZ-3B third stage.

In Figure 8 and Figure 9 are shown dark flight paths of all seventeen fragments. Figure 8 depicts evolution of altitude as a function of time, while Figure 9 depicts altitude as a function of downrange.

A decelerated, non-ablating object can stay in the atmosphere for many minutes and travel a significant distance from its terminal point. It closely follows the original observed direction of the flight. Fragments impacting the surface are generally distributed according to their mass (more massive objects decelerate less and reach further). The width of the impact area is affected by the wind and less significantly by the Earth's rotation. Geodetic positions of the impacting fragments are shown in Figure 10 (colored filled circles) together with projections of the luminous and dark flight trajectories onto a world map and the locations of the observing stations. The simulated im-

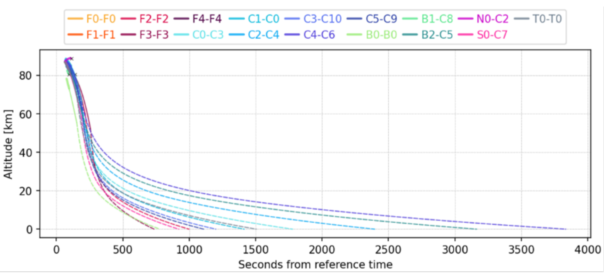

Figure 8: Simulated dark flight altitude evolution against time. Thicker lines belong to the observed portions of the trajectories. Thinner lines depict how trajectories continued after observations until the terminal points (v = 3 km/s). Dashed lines belong to the dark flight data.

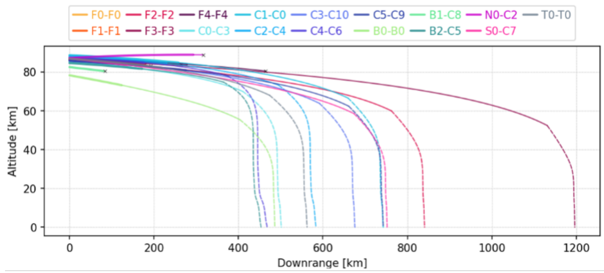

Figure 9: Simulated dark flight altitude evolution against downrange. Thicker lines belong to the observed portions of the trajectories. Thinner lines depict how trajectories continued after observations until the terminal points (v = 3 km/s). Dashed lines belong to the dark flight data.

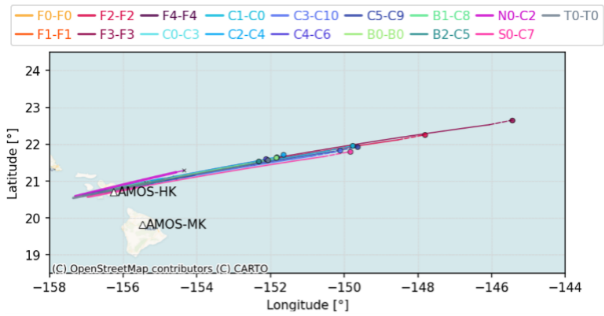

Figure 10: Simulated luminous and dark flight trajectories projected onto world map and impact locations of the surviving fragments (circles). Thicker lines belong to the observed portions of the trajectories. Thinner lines depict how trajectories continued after observations until the terminal points (v = 3 km/s). Dashed lines belong to the dark flight data.

pact area is approximately 720 km long. The fragments impacted into the Pacific Ocean around 430 km northwest of the Hawaiian Islands.

4. EVENT RECONSTRUCTION AND ANALYSIS WITH DRAMA

Previous work provided all the necessary datasets, including measurements and simulations, which were used as inputs for the final DRAMA simulations. To refine the DRAMA simulations, two specific points were selected: video recording and measurements of the initial CZ-3B breakup (occurring at 2020-10-25T08:00:36.1, as depicted in Figure 12) and measurements from the intersection of all fragments at 2020-10-25T08:02:02.5 (as shown in Figure 11), when the highest number of fragments were triangulated.

From the triangulated trajectories obtained from AMOS measurements, we have access to fragments' masses, positions, velocities, and decelerations in Earth-centered Earth-fixed (ECEF) coordinates. These data were utilized for comparison with DRAMA simulations. The pri-

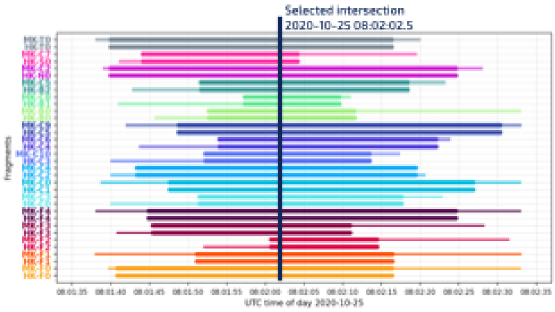

Figure 11: Time scales of measured fragments from AMOS CZ-3B re-entry event observation. Narrower part of the line shows part, when observations were acquire from only single camera or cannot be associated with fragment from second camera; Wider line parts show parts of the trajectory, when triangulation was successfull. Vertical line shows the time, which was selected reference point for further DRAMA simulation finetuning.

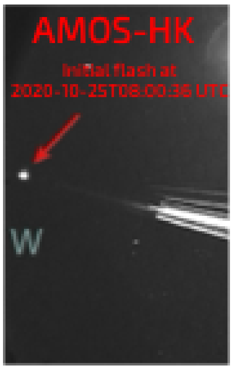

Figure 12: Moment of the fragmentation recorded at 2020-10-25T08:00:36 at position azimuth 258.34 deg and elevation 8.51 deg.

mary objective of the simulations was to optimize the DRAMA input parameters (primarily orbital elements) to ensure that simulations align with two selected points from AMOS measurements to the greatest extent possible.

As a rapid comparison tool, a polar plot of the composite locations of DRAMA fragments with the AMOS composite measurement figure as a background (Figure 13, left) was selected. This visualization demonstrates the trajectory of the fragments across the local sky during the AMOS-HK observation. Additionally, Figure 13, right presents a comparison between the AMOS recorded location of the main breakup and the DRAMA simulated location.

The initial visual inspection (see Figure 13) of the simulated trajectories of fragments towards the composite AMOS image reveals a satisfactory alignment between the DRAMA simulation and the AMOS observation. The residual angular offset in the primary break-up location in AMOS-HK horizontal coordinates was 1.6 degrees, and

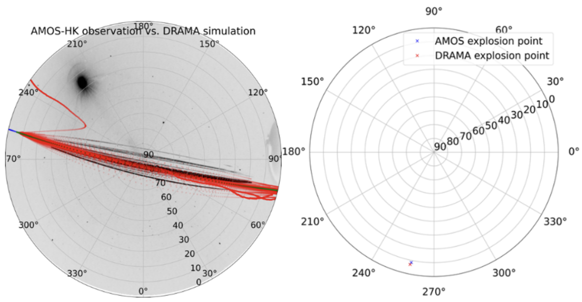

Figure 13: Left: Polar comparison of the AMOS composite image with all fragments' trajectories generated during the run; Right: Comparison of the break-up location in AMOS-HK horizontal coordinates. Results obtained using refined DRAMA configuration.

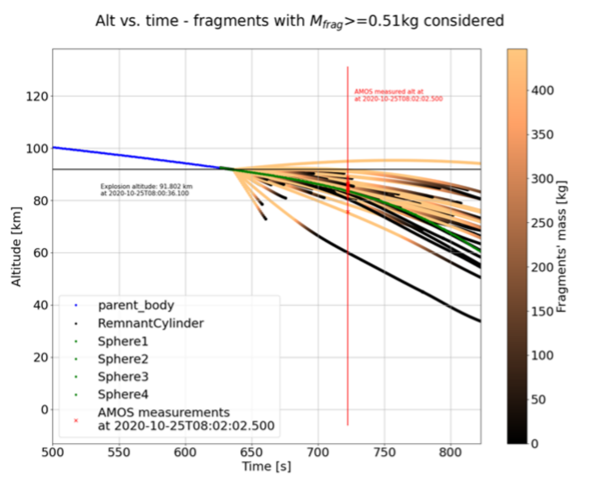

Figure 14: Drama run simulated fragments and their altitude vs. Time dependence compared with altitude of observed AMOS fragments at 2020-10-25T08:02:02.5. Color scale depicts the current mass at specific time i.e., mass loss is depicted. Results obtained using refined DRAMA configuration.

the time offset was less than 0.1 second. Assuming that DRAMA generates the initial fragment positions after the explosion with a time step of 0.1 second, this represents the inherent accuracy limit of the DRAMA simulation. These residuals were achieved through refinements in the input orbital elements and explosion trigger altitude. The explosion trigger utilized for these simulation runs was set to an altitude of 91,850 km, which is realistic, although 10 km higher than the expected value based on published literature [12]. Conversely, lower break-up triggers resulted in the absence of any explosion. In Figure 14 is shown the resulting simulated fragments distribution, time vs altitude.

Figure 15 and 16 present comparisons between the velocity and deceleration versus altitude dependencies of DRAMA-simulated fragments in relation to AMOS-recorded values. As previously reported, these values ex-

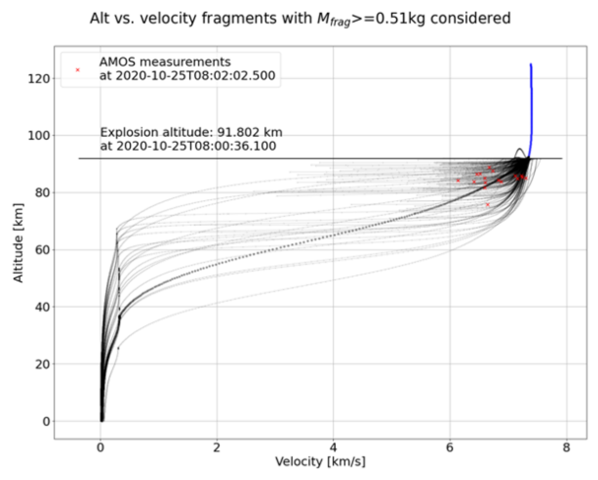

Figure 15: Velocity of DRAMA fragments comparison with amos observed data. Only observable fragments (m¿0.51kg) are considered. Results obtained using refined DRAMA configuration.

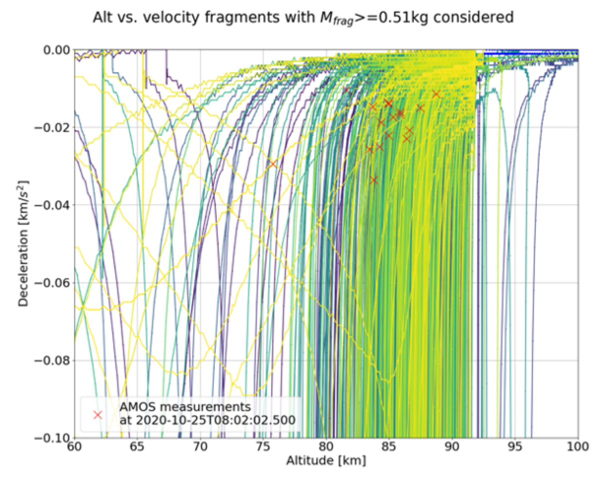

Figure 16: Deceleration of DRAMA fragments comparison with amos observed data. Only observable fragments (m¿0.51kg) are considered. Results obtained using refined DRAMA configuration.

hibit a good fit with the initial DRAMA simulations. Notably, AMOS measurements closely align with the predicted intervals by DRAMA.

Figure 17 presents the estimated impact regions by DRAMA and AMOS dark flight analysis. Both regions are centered at the same location. However, DRAMA generates significantly more fragments, resulting in a simulated impact region that is approximately twice larger than the AMOS impact region. Furthermore, the longitude and latitude densities between the DRAMA and AMOS impact regions exhibit a satisfactory correlation.

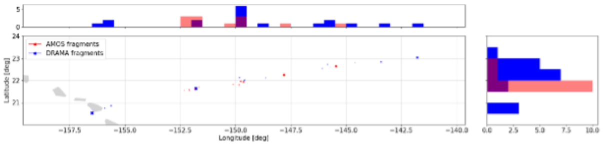

Figure 17: Comparison of the impact locations as predicted by AMOS nominal processing and DRAMA tool. Results obtained using refined DRAMA configuration. Side histograms depicts the density of impacting fragments along latitude and longitude.

In accordance with the outcomes of the initial DRAMA simulation run, the mass distributions are presented in Figure 18. To facilitate a more precise comparison, we have established an equal bin size for both histograms. As evident from the figure, both distributions exhibit an exponential trend, with the DRAMA case exhibiting a significantly steeper slope. This indicates that DRAMA is generating a higher number of fragments with masses within the interval (0.01-0.1) kg, which are beyond the detection capabilities of AMOS cameras. Conversely, there are five fragments with masses exceeding 100kg, which should be sufficiently compact to be observed in AMOS recordings. However, AMOS reported the maximum mass of any fragment as 51.5kg.

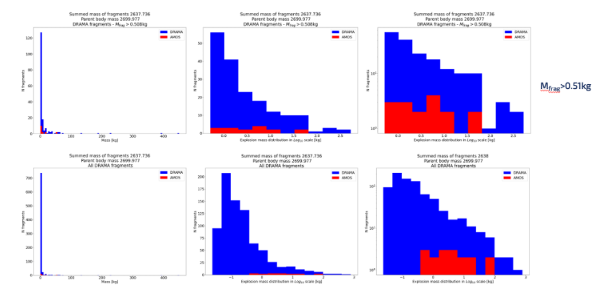

Figure 18: Mass distribution comparison between DRAMA and AMOS observed fragments. Upper row considers only observable fragments (m¿0.51kg); bellow row considers all DRAMA generated fragments. Equal binning size – 5 kg per bin for the whole interval of mass for both systems. Results obtained using refined DRAMA configuration.

The comparison between break-up velocity distributions from DRAMA and AMOS is presented in Figure 19. Both distributions exhibit an exponential trend, with the DRAMA fragments exhibiting a steeper slope, primarily attributed to the selection bias observed in the AMOS data. Notably, the maximum delta velocity recorded in the simulated data is approximately 1.4 km/s. Furthermore, the absolute averaged delta velocity values for the event reported by DRAMA are significantly higher than those recorded by AMOS cameras, approximately three

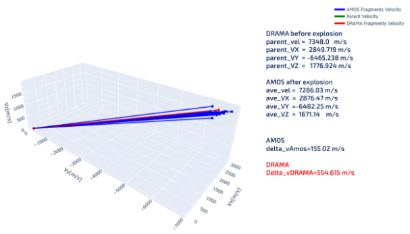

Figure 19: Comparison of the velocity vectors after the break-up event. Depicted are also averaged cartesian velocities and nominal delta velocity as observed from AMOS and estimated by DRAMA. Results obtained using refined DRAMA configuration.

times greater. This discrepancy is likely due to the assumption made by DRAMA that an explosion occurred during the break-up, as the explosion parameter cannot be disabled in the DRAMA GUI. These results represent the most accurate event reconstruction available at present.

5. CONCLUSIONS

Data reduction and fragment estimation have been conducted using AMOS data. Data reduction required several changes, mostly toward the fragment association and trajectory reconstruction. Also, experimental processing using novel programming methods has been exploited. Finally, seventeen of the fragments have been associated between recordings, and almost 60 seconds of the event have been reconstructed. For these fragments, the estimated values have been: flight duration, initial altitude, final attitude, distance from the observer, downrange, downrange average speed, initial velocity, final velocity, initial deceleration, final deceleration, and mean absolute magnitude. These parameters have been used to estimate the ablation coefficient and survivability of each of the fragments. Furthermore, the results suit as a baseline for comparison with DRAMA simulations.

The comprehensive analysis of the CZ-3B re-entry event using DRAMA and AMOS data has significantly enhanced our understanding of break-up events. Through refinement of DRAMA simulations, incorporating AMOS ground-based observations, we achieved a high level of alignment (1.6 degree offset in break-up location and 0.05-degree angular offset of fragments' cloud COM) with observed data, despite the inherent challenges of modeling such complex events. The exercise highlighted crucial insights, particularly concerning the discrepancies in mass and velocity distributions between the simulated and observed fragments.

The refined DRAMA configuration, developed through iterative adjustments of input parameters, proved effective in reconstructing the trajectory and impact regions of the re-entry fragments. The use of multiple simulation runs facilitated a broader statistical analysis, which underpinned the development of a more accurate and reliable reconstruction of the event.

Lessons learned from this exercise underscore the importance of addressing selection biases in the modeling process, particularly in the context of large-scale, high-fidelity simulations. Future efforts should focus on enhancing DRAMA's configuration, especially regarding explosion parameter settings, to better simulate low-energy break-up events. Furthermore, continued collaboration with observational networks like AMOS is imperative to refine modeling approaches and validate simulation outputs.

Last but not least, we dedicated effort to better understand how to improve the initial conditions which may contribute to the future events modeling by exploiting orbit determination and improvement topics, as well as focusing on the attitude estimation and attitude evolution of cylindrical upper stages, common objects re-entering the atmosphere. Analyzed were several different upper stages, their orbits, and attitude. The majority were present on highly eccentric orbits. The results were reported partially in this report.

ACKNOWLEDGMENTS

The entirety of the study and activity was funded under the European Space Agency's Plan for European Cooperating States (ESA PECS) 6 call for proposals in Slovakia under the European Space Agency Contract No. SK6_26-4000136672/21/NL/SC. We would like to express our sincere gratitude to all the partners who provided valuable assistance to the activity, including the Astronomical Institute of the University of Bern, Switzerland, and Cilium Engineering Sp. z o. o., Poland.

REFERENCES

1. MARTIN, C. E., et al. Introducing the ESA DRAMA tool. In: 55th International Astronautical Congress of the International Astronautical Federation, the International Academy of Astronautics, and the International Institute of Space Law. 2005. p. IAA. 5.12. 3.04.

2. DRAMA GUI 3.1.1 – DRAMA software user manual; REF: GEN-SW-SUM-00342-OPS-SD, Issue: 2.5; Date: 07/10/2024 `https://sdup.esoc.esa.int/drama/downloads/documentation/DRAMA-Software-User-Manual.pdf`

3. ŠILHA, Jiří, et al. Analysis of re-entry event of CZ-3B R/B observed by all-sky meteor cameras AMOS. In: 2nd NEO and Debris Detection Conference. 2023. p. 12.

4. Hill, K. A., Rogers, L. A., and Hawkes, R. L. High geocentric velocity meteor ablation. Astronomy and Astrophysics, 444(2):615-624, 2005.

Table 2: Dark flight simulation input and resulting values: duration of the dark flight t_f, impact velocities v_f and impact kinetic energies K_f.

Fragment	H_T *[km]*	m_T *[kg]*	k_c *[-]*	*A* *[-]*	Γ *[-]*	ρ *[kg/m3]*	r_c *[m]*	t_f *[min]*	v_f *[m/s]*	K_f *[J]*
F0-F0						*Demise*				
F1-F1						*Demise*				
F2-F2	59.901	51.452	0.010	31.554	0.610	4000	74.26	13.0	20.100	10394.01
F3-F3	52.355	51.488	0.040	12.522	0.608	4000	46.79	8.0	31.982	26332.45
F4-F4						*Demise*				
C0-C3	69.948	0.544	0.015	24.080	0.609	3000	15.66	27.0	9.792	26.06
C1-C0	66.489	16.306	0.007	40.024	0.610	2700	65.00	20.4	12.922	1361.23
C2-C4	73.050	0.079	0.010	31.554	0.610	4500	8.22	37.3	7.092	1.98
C3-C10	63.790	2.803	0.020	19.878	0.609	4000	22.34	16.9	15.598	340.96
C4-C6	77.857	0.003	0.010	31.554	0.610	5000	2.73	61.4	4.308	0.03
C5-C9	62.321	15.914	0.010	31.554	0.610	4500	48.28	15.3	17.192	2351.73
B0-B0	55.369	3.604	0.100	6.798	0.606	3000	15.64	10.4	25.370	1159.82
B1-C8						*Demise*				
B2-C5	74.680	0.001	0.050	10.791	0.608	2700	1.50	50.3	5.257	0.02
S0-C7	58.477	4.390	0.030	15.169	0.609	5500	20.38	12.2	21.415	1006.61
T0-T0	67.906	5.299	0.005	50.088	0.610	5000	40.71	22.5	11.764	366.67
N0-C2						*Demise*				

5. Weryk, R. and Brown, P. Simultaneous radar and video meteors II: Photometry and ionisation. Planetary and Space Science, 81:32-47, 2013.

6. Borovička, J. et al. Two strengths of ordinary chondritic meteoroids as derived from their atmospheric fragmentation modeling. The Astronomical Journal, vol. 160, no. 1, 2020.

7. Ceplecha, Z., Borovička, J., Elford, W.G. et al. Meteor phenomena and bodies. Space Science Reviews, 84:327-471, 1998.

8. Paprskárová, M. Fragmentation of fireballs and their dust clouds in the atmosphere. Diploma thesis, Comenius University in Bratislava, 2023.

9. Jansen-Sturgeon, T. et al. A dynamic trajectory fit to multisensory fireball observations. The Astronomical Journal, 160(4):190, 2020.

10. Baláž, M. Determination of total meteoroid flux in milimetre to metre size range. Diploma thesis, Comenius University in Bratislava, 2018.

11. Carter, R., Jandir, P., and Kress, M. Constraining the drag coefficients of meteors in dark flight. Meteoroids: The smallest solar system bodies Conference, 2011.

12. LEMMENS, Stijn, et al. Planned yet uncontrolled reentries of the cluster-ii spacecraft. In: Seventh European Conference on Space Debris. 2017.

13. JOHNSON, Nicholas L., et al. NASA's new breakup model of EVOLVE 4.0. Advances in Space Research, 2001, 28.9: 1377-1384.

14. William Jones , Ian Halliday, Effects of excitation and ionization in meteor trains, Monthly Notices of the Royal Astronomical Society, Volume 320, Issue 4, February 2001, Pages 417–423, https://doi.org/10.1046/j.1365-8711.2001.03833.x